ISBN: 978-3-95450-262-2 ISSN: 2673-5350 doi: 10.18429/JACoW-IBIC2025-MOPMO28

UV–VIS EMISSIONS FROM HIGH ENERGY HEAVY IONS: MECHANISMS AND APPLICATIONS TO SINGLE-ION DETECTION

R. Ghagi*,[1], R. Singh, P. Boutachkov, B. Walasek-Hoehne, GSI, Darmstadt, Germany
H. Zhang, C. Welsch, University of Liverpool, Liverpool, UK
[1] also at University of Liverpool, Liverpool, UK

Abstract

We investigate two well known ultraviolet–visible (UV–VIS) photon emission processes from highly charged uranium ions with energies of 300- 700 MeV/u. By combining theoretical models with estimates from the literature, we evaluate fluorescence yields from air and transition radiation from surfaces. Experimental studies with slow-extracted U^{73+} beam at the high-energy beam transport line at GSI–FAIR confirm the feasibility of single-ion detection, with prototype detectors achieving up to 99.5 % efficiency. These findings suggest UV–VIS emission as a robust method for fast, radiation-hard single-particle counting.

INTRODUCTION

High-energy, high-intensity heavy-ion beams are essential tools for exploring new physics and probing fundamental interactions at facilities such as GSI–FAIR [1]. Reliable, fast, and radiation-hard diagnostics, capable of sustained performance over extended periods, are essential prerequisites for their successful operation. In this paper, we summarize the primary mechanisms of UV–VIS emission from relativistic heavy ions in air and on metallic targets, and highlight the development and testing of a prototype detector that harnesses this emission for efficient, radiation-hard particle counting.

BEAM-INDUCED FLUORESCENCE

Beam-induced fluorescence (BIF) in pure gases is a well-established phenomenon [2] with wide applications in beam diagnostics [3, 4]. Air fluorescence studies with electrons over a wide energy range of 500 keV to 50 GeV [5–8], with protons at 120 GeV [9], and with 0.3–5.1 MeV α-particles in radioluminescence studies [10], reports a yield of $\approx$ 20 photons per MeV of energy deposited in air in the 300–420 nm band under conditions close to normal temperature and pressure (NTP).

Air fluorescence at atmospheric pressure (1013.25 hPa) is dominated by the second positive (2P) system[1] of N_2, with only a small contribution from the first negative (1N) system of N_2^+. Within the 2P system, the 2P(0,0) band at 337.1 nm is the strongest single feature, accounting for $\approx$ 25 % of the yield, while many other 2P bands together contribute far more than the 1N(0,0) band at 391.4 nm [5, 12].

Collisional quenching, i.e. non-radiative de-excitation of excited molecules by collisions, reduces both the fluorescence yield and the radiative lifetime. In air, the fluorescence yield increases with pressure due to higher molecular density, but this is counteracted by quenching. For a given gas composition, the pressure dependence of the yield for a $v \to v'$ transition, $Y_{vv'}(P)$, and of the corresponding excited-state lifetime $\tau_v(P)$, is described by the Stern–Volmer equation [11, 13]:

$$\frac{Y_{vv'}(P)}{Y^0_{vv'}} = \frac{\tau_v(P)}{\tau^0_v} = \frac{1}{1+P/P^0_v}, \quad (1)$$

where $Y^0_{vv'}$ and τ^0_v are the radiative yield and lifetime of the $v \to v'$ transition in the absence of quenching. The parameter P^0_v is the characteristic Stern–Volmer pressure of state v, defined as the pressure at which collisional quenching and radiative decay occur with equal probability. For the $2P(0, v'')$ and $1N(0, v'')$ transitions in air, the values are $P^0 = 15.3$ hPa and $P^0 = 1.2$ hPa, respectively. At atmospheric pressure (1013.25 hPa), the corresponding quenching factors, $1 + P/P^0_v$, are 67.2 and 845.4. Thus, quenching reduces the lifetime of the 337.1 nm band from 38.9 ns to 0.57 ns, and that of the 391.4 nm band from 65.2 ns to 77 ps. These values have been experimentally confirmed for the 2P system, whereas the very low yield of the 391.4 nm band and the presence of neighboring 2P bands (e.g. 380.5 nm and 399.8 nm) present practical challenges for accurate lifetime measurements of the 1N system [13].

Apart from collisional quenching, the dominance of the 2P system in atmospheric air is further reinforced by a significant fraction of N_2^+ converting to excited 2P states of N_2 rather than emitting via the 1N system [2, 14]. The dominant pathway for this re-population of $N_2(C^3\Pi_u)$ in the 2P system proceeds via the formation of N_4^+, followed by dissociative recombination with an electron [15].

As fluorescence is driven mainly by cascades of low-energy secondary electrons generated during ionization by the primary charge, precise calculation of their energy deposition is essential for reliable estimates of the photon yield in any experimental geometry [14]. For the present study, we estimate the number of photons for the experimental ion beams (Table 1) by calculating the energy lost by primary ions using the Bethe–Bloch formula and assuming a geometry in which all of this energy loss is deposited in the medium.

* r.ghagi@liverpool.ac.uk

[1] The second positive (2P) system refers to electronic transitions in neutral nitrogen, $N_2(C^3\Pi_u \to B^3\Pi_g)$, while the first negative (1N) system corresponds to transitions in the nitrogen ion, $N_2^+(B^2\Sigma_u^+ \to X^2\Sigma_g^+)$ [11]. Individual bands are denoted as $2P(v, v')$ or $1N(v, v')$, where v and v' are the vibrational quantum numbers of the upper and lower states, respectively. For example, the 2P(0,0) band at 337.1 nm arises from the $v = 0 \to v' = 0$ transition of neutral N_2, while the 1N(0,0) band at 391.4 nm corresponds to the analogous transition in N_2^+.

ISBN: 978-3-95450-262-2 ISSN: 2673-5350 doi: 10.18429/JACoW-IBIC2025-MOPMO28

TRANSITION RADIATION

Transition radiation (TR) is the electromagnetic radiation emitted when a charged particle moves across an optically inhomogeneous region like the interface between two media with different dielectric properties. Optical transition radiation (OTR) i.e., TR in the visible range was proposed for beam diagnostics in 1973 [16] and has since become widely used technique. Extensive studies have quantified how the yield, polarization, and angular/spectral distributions depend on incidence and observation angles, energy, radiator material, surface roughness, and wavelength [16–18].

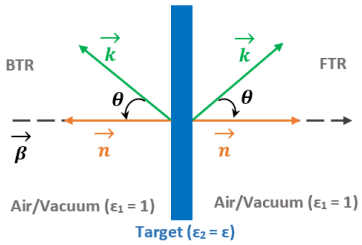

Figure 1: Charged particle beam incident normally on the target.

The spectral–angular intensity of backward transition radiation (BTR) for a particle of charge Ze and velocity $\vec{\beta} = \vec{v}/c$ crossing at normal incidence from vacuum ($\varepsilon_1 = 1$) into a medium with dielectric constant $\varepsilon_2 = \varepsilon$, as shown in Fig. 1, is given in the literature [19]; by substituting $d\omega = \frac{2\pi c}{\lambda^2}\, d\lambda$, $d\Omega = \sin\theta\, d\theta\, d\phi$, and dividing by the photon energy hc/λ, the corresponding double differential photon yield can be written as:

$$dN(\lambda,\theta) = \frac{Z^2 e^2 \beta^2 \sin^3\theta \cos^2\theta |1-\varepsilon|^2}{\pi \varepsilon_0 hc\lambda \left(1-\beta^2\cos^2\theta\right)^2}\, d\lambda\, d\theta \times \left| \frac{\left(1+\beta\sqrt{\varepsilon-\sin^2\theta}-\beta^2\right)}{\left(1+\beta\sqrt{\varepsilon-\sin^2\theta}\right)\left(\sqrt{\varepsilon-\sin^2\theta}+\varepsilon\cos\theta\right)} \right|^2 . \quad (2)$$

The radiation is linearly polarized in the plane of observation (spanned by the surface normal $\vec{n}$ and observation direction $\vec{k}$) and, for normal incidence, is azimuthally symmetric. The formula for forward TR (FTR, emitted into medium 2) follows from Eq. (2) by the usual substitution $\beta \to -\beta$. For normal incidence, BTR and FTR have essentially identical spectral and angular distribution.

Using tabulated optical constants of Al, we calculate the dielectric function $\varepsilon(\lambda) = (n(\lambda) + \mathrm{i}\,k(\lambda))^2$ [20]. Integrating Eq. (2) over θ, we obtain the UV–VIS photon spectrum, and an additional integration over λ in the range 300–700 nm gives the photon yield estimates, which are summarized in Table 1. By integrating only over λ, we obtain the angular distribution of TR, as shown in Fig. 2. In contrast to fluorescence, which is isotropic, TR exhibits a characteristic angular distribution that depends on the ion energy, the target surface geometry, and the angle of incidence.

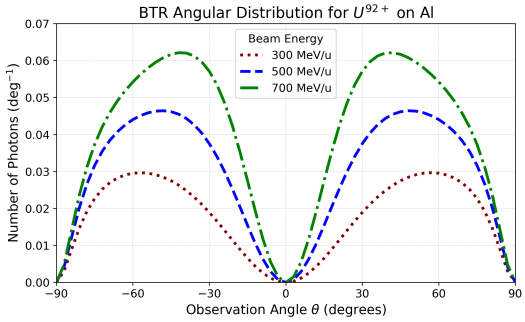

Figure 2: OTR angular distribution.

Table 1: Calculated Yields (300–700 nm) for $\mathbf{U^{92+}}$ in Air

T (MeV/u)	Energy deposited (MeV/mm)	Fluorescence photons (mm^{-1})	TR photons per surface
300	≈ 3.2	≈ 63	≈ 7.9
500	≈ 2.5	≈ 49	≈ 12.4
700	≈ 2.2	≈ 44	≈ 16.4

RESULTS AND DISCUSSION

First experiments were performed to demonstrate a proof-of-concept ion detector based on UV–VIS emissions. Two detector configurations were studied in ambient air (NTP). Detector A consisted of a 5 × 5 × 5 cm^3 empty paper box with a 1 × 3 cm^2 window through which the PMT observed the signal perpendicular to the beam path. Detector B consisted of a stack of 100 aluminum foils, each 18 µm thick, separated by 0.1 mm gaps; the spacing was chosen to ensure that the OTR yield exceeded that from air fluorescence as evident later in the text. The detectors were coupled to a Hamamatsu R6427 PMT and operated in coincidence with a standard BC400 scintillator providing the trigger signal. Signals were recorded with a Tektronix MSO58 oscilloscope. A schematic of the experimental setup is shown in Fig. 3. The setup was placed 90 cm downstream of the exit flange in air, corresponding to beam energies at the detectors of approximately 288, 491, and 692 MeV/u. The interaction with exit flange material followed by the air path were sufficient for the ions to reach their equilibrium charge state of ≈ 91.

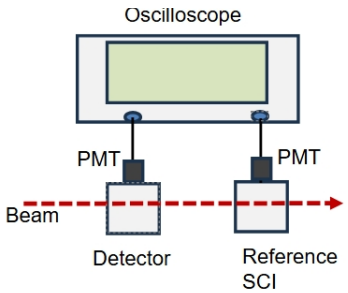

Figure 3: Schematics of Experimental Setup.

The corresponding amplitude distributions are shown in Fig. 4, where each histogram is annotated with the sample mean, standard deviation, and the number of ions detected out of 10^4 shots. Insets display representative single-ion

ISBN: 978-3-95450-262-2 ISSN: 2673-5350 doi: 10.18429/JACoW-IBIC2025-MOPMO28

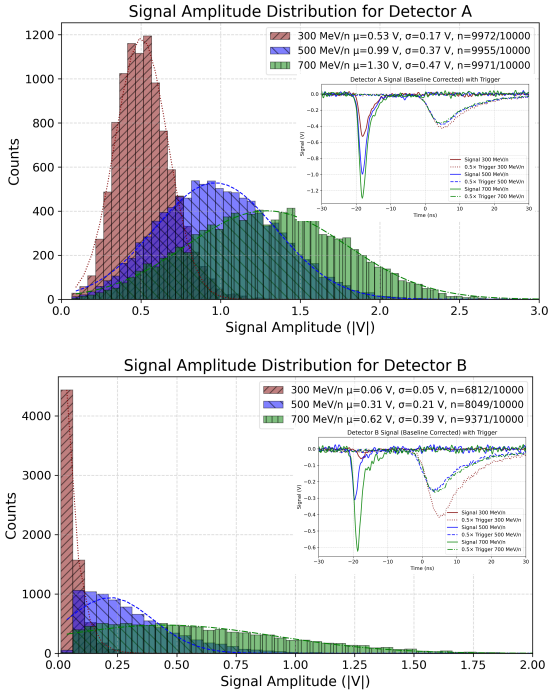

Figure 4: Signal Amplitudes Distribution for Detectors A (top) and B (bottom). Insets: typical detector and trigger waveforms for a single ion.

waveforms with amplitudes close to the sample mean. On average, four detected photons produced a pulse of 30 mV at the chosen PMT settings. A threshold corresponding to six times the noise standard deviation was applied to the detector signals for ion counting. For Detector A, the single-ion *detection efficiency* exceeded 99.5 % at all beam energies. Both the mean signal amplitude and its spread increased with energy. For Detector B, the efficiencies were 68.1 %, 80.5 %, and 93.7 % at 300, 500, and 700 MeV/u, respectively, with the mean amplitudes and standard deviations likewise increasing with energy. Figure 5 summarizes the timing characteristics of the detectors. The left and right histograms show, respectively, the distribution of the relative time difference between the detector-signal peak (negative) and the 50 % of falling edge of the reference scintillator (trigger) signal, and the distribution of the signal full width at half maximum (FWHM). For Detector A, the mean arrival times vary within 0.2 ns, consistent with the expected delay for ions traversing ≈ 20 cm between the detector and the reference scintillator at 300–700 MeV/u. The measured FWHM values are around 2.56 ns, also broadly in agreement with the characteristic PMT rise time of 1.7 ns and the fluorescence lifetime of the dominant 2P line, 0.57 ns. The broader distributions observed for Detector B are attributed to the much smaller signal amplitudes (low signal-to-noise ratio), complex interactions of charges with alternating foils and air gaps, and additional dispersion introduced during signal transport through narrow gaps.

Estimates of the number of photons from air fluorescence, summarized in Table 1, decrease with energy in the 300–700 MeV/u range, reflecting the Bethe–Bloch $1/\beta^2$ trend which is in contradiction to the observations to detector

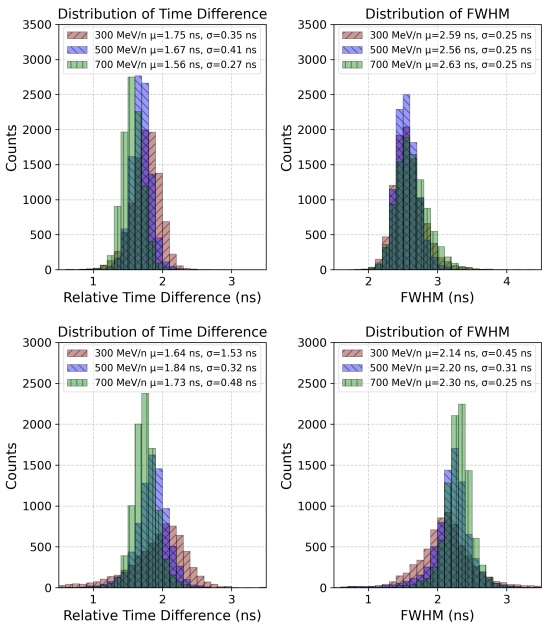

Figure 5: Timing Characteristics for detectors A (top) and B (bottom).

A. Although some OTR contribution from the paper interface is expected for detector A, this cannot account for all the UV-VIS yield increase with ion energy. For Detector B, the per-cell OTR yields are 15.8, 24.7, and 32.7 photons at 300, 500, and 700 MeV/u, respectively, while fluorescence from the 0.1 mm air gaps contributes an additional 6.3, 4.9, and 4.4 photons per gap. Optical modeling of the detector geometry and angular distributions of sources indicates an overall transport efficiency of only ≈1% of OTR photons to the PMT with the remainder lost to multiple reflections. The BIF photons reaching the PMT in this geometry would be negligible owing to isotropic emissions.

It is evident that the simple description of ion-induced air fluorescence based on cited empirical studies are inadequate to explain our photon yield observations from detector A. It appears that a detailed modeling of secondary and cascade electrons in the detector volume covering all the relevant chemical pathways needs to be included e.g. ionization quenching [21]. In addition, contributions from other neglected radiation channels such as polarization Bremsstrahlung [22] and secondary-electron Bremsstrahlung [23–25] has to be quantitatively assessed. Nevertheless, these proof-of-concept experiments with prototype detector assemblies demonstrate robust single-ion detection efficiencies validating the approach to be applicable for fast, radiation-hard single particle counting both in air (detector A) and vacuum (detector B).

ACKNOWLEDGMENTS

This work is supported by the STFC Liverpool Centre for Doctoral Training for Innovation in Data Intensive Science (LIV.INNO) under grant agreement ST/W006766/1, and by the GSI/FAIR Innovation Fund. We thank Marco Biljan and Michael Müller for extensive help in preparation of the experiment, and Peter Forck for valuable discussions on BIF.

ISBN: 978-3-95450-262-2 ISSN: 2673-5350 doi: 10.18429/JACoW-IBIC2025-MOPMO28

REFERENCES

[1] M. Durante *et al.*, "All the fun of the FAIR: fundamental physics at the facility for antiproton and ion research", *Phys. Scr.*, vol. 94, no. 3, p. 033001, 2019. doi:10.1088/1402-4896/aaf93f

[2] R. Hampf, J. Wieser, and A. Ulrich, "Light emission processes in the context of optical beam profile monitors", *Eur. Phys. J. D*, vol. 77, no. 3, p. 51, 2023. doi:10.1140/epjd/s10053-023-00624-6

[3] F. Becker, C. Andre, P. Forck, D. Hoffmann, and H. Iwase, "Profile measurement by beam induced fluorescence for 60 to 750 MeV/u heavy ion beams", in *Proc. EPAC'06*, Edinburgh, UK, Jun. 2006, paper TUPCH010, pp. 1013–1015.

[4] I. Yamada, M. Wada, K. Moriya, J. Kamiya, P. K. Saha, and M. Kinsho, "High-intensity beam profile measurement using a gas sheet monitor by beam induced fluorescence detection", *Phys. Rev. Accel. Beams*, vol. 24, no. 4, p. 042801, 2021. doi:10.1103/PhysRevAccelBeams.24.042801

[5] J. Rosado, F. Blanco, and F. Arqueros, "On the absolute value of the air-fluorescence yield", *Astropart. Phys.*, vol. 55, pp. 51–62, 2014. doi:10.1016/j.astropartphys.2014.02.003

[6] M. Nagano, K. Kobayakawa, N. Sakaki, and K. Ando, "New measurement on photon yields from air and the application to the energy estimation of primary cosmic rays", *Astropart. Phys.*, vol. 22, no. 3-4, pp. 235–248, 2004. doi:10.1016/j.astropartphys.2004.08.002

[7] P. Colin *et al.*, "Measurement of air and nitrogen fluorescence light yields induced by electron beam for uhecr experiments", *Astropart. Phys.*, vol. 27, no. 5, pp. 317–325, 2007. doi:10.1016/j.astropartphys.2006.11.008

[8] R. Abbasi *et al.*, "Air fluorescence measurements in the spectral range 300–420 nm using a 28.5 GeV electron beam", *Astropart. Phys.*, vol. 29, no. 1, pp. 77–86, 2008. doi:10.1016/j.astropartphys.2007.11.010

[9] M. Ave *et al.*, "Precise measurement of the absolute fluorescence yield of the 337 nm band in atmospheric gases", *Astropart. Phys.*, vol. 42, pp. 90–102, 2013. doi:10.1016/j.astropartphys.2012.12.006

[10] J. Sand, S. Ihantola, K. Peräjärvi, H. Toivonen, and J. Toivonen, "Radioluminescence yield of alpha particles in air", *New J. Phys.*, vol. 16, no. 5, p. 053022, 2014. doi:10.1088/1367-2630/16/5/053022

[11] F. Arqueros, F. Blanco, and J. Rosado, "Analysis of the fluorescence emission from atmospheric nitrogen by electron excitation, and its application to fluorescence telescopes", *New J. Phys.*, vol. 11, no. 6, p. 065011, 2009. doi:10.1088/1367-2630/11/6/065011

[12] M. Ave *et al.*, "Measurement of the pressure dependence of air fluorescence emission induced by electrons", *Astropart. Phys.*, vol. 28, no. 1, pp. 41–57, 2007. doi:10.1016/j.astropartphys.2007.04.006

[13] T. Waldenmaier, J. Blümer, D. Gonzalez, and H. Klages, "Measurement of the air fluorescence yield with the airlight experiment", *Nucl. Instrum. Methods Phys. Res. A*, vol. 597, no. 1, pp. 67–74, 2008. doi:10.1016/j.nima.2008.08.047

[14] F. Blanco and F. Arqueros, "The role of secondary electrons in some experiments determining fluorescence emission from nitrogen $C^3\Pi_u$ levels", *Phys. Lett. A*, vol. 345, no. 4-6, pp. 355–361, 2005. doi:10.1016/j.physleta.2005.07.059

[15] H. Xu, A. Azarm, J. Bernhardt, Y. Kamali, and S. Chin, "The mechanism of nitrogen fluorescence inside a femtosecond laser filament in air", *Chem. Phys.*, vol. 360, no. 1-3, pp. 171–175, 2009. doi:10.1016/j.chemphys.2009.05.001

[16] L. Wartski, J. Marcou, and S. Roland, "Detection of optical transition radiation and its application to beam diagnostics", *IEEE Trans. Nucl. Sci.*, vol. 20, no. 3, pp. 544–548, 1973. doi:10.1109/TNS.1973.4327172

[17] R. Singh, T. Reichert, and B. Walasek-Hoehne, "Optical transition radiation based transverse beam diagnostics for nonrelativistic ion beams", *Phys. Rev. Accel. Beams*, vol. 25, no. 7, p. 072801, 2022. doi:10.1103/PhysRevAccelBeams.25.072801

[18] S. Borovkov, S. Grishenkov, V. Novikov, E. Serga, A. Kharlamov, and Y. S. Khodyrev, "On studying a possibility to use optical transition radiation for proton beam diagnostics", *Nucl. Instrum. Methods Phys. Res. A*, vol. 294, no. 1-2, pp. 101–107, 1990. doi:10.1016/0168-9002(90)91828-Y

[19] M. L. Ter-Mikaelian, *High-energy electromagnetic processes in condensed media*. John Wiley & Sons, 1972.

[20] M. N. Polyanskiy, "Refractiveindex. info database of optical constants", *Sci. Data*, vol. 11, no. 1, p. 94, 2024. doi:10.1038/s41597-023-02898-2

[21] N. Lepikhin, A. Klochko, N. Popov, and S. Starikovskaia, "Long-lived plasma and fast quenching of N_2 ($C^3\Pi_u$) by electrons in the afterglow of a nanosecond capillary discharge in nitrogen", *Plasma Sources Sci. Technol.*, vol. 25, no. 4, p. 045003, 2016. doi:10.1088/0963-0252/25/4/045003

[22] M. Y. Amusia, "'Atomic Bremsstrahlung': retrospectives, current status and perspectives", *Radiat. Phys. Chem.*, vol. 75, no. 10, pp. 1232–1250, 2006. doi:10.1016/j.radphyschem.2006.04.009

[23] R. M. Ferro, A. Mangiarotti, and J. M. Fernandez-Varea, "Calculation of secondary electron bremsstrahlung in the binary encounter approximation using dirac–hartree–fock–slater velocity distributions", *Nucl. Instrum. Methods Phys. Res. B*, vol. 478, pp. 70–79, 2020. doi:10.1016/j.nimb.2020.05.008

[24] I. Al Samarai, O. Deligny, and J. Rosado, "The small contribution of molecular bremsstrahlung radiation to the air-fluorescence yield of cosmic ray shower particles", *Astropart. Phys.*, vol. 83, pp. 1–5, 2016. doi:10.1016/j.astropartphys.2016.06.006

[25] V. Kas'yanov and A. Starostin, "On the theory of bremsstrahlung of slow electrons on atoms", *Sov. Phys. JETP*, vol. 21, no. 193, p. 15, 1965.